Inelastic scattering of 28.0 MeV protons on ^{56}Fe

A. Kumar,[1] D. K. Avasthi,[2] A. Tripathi,[2] S. K. Datta,[2] and I. M. Govil[1]
[1]*Department of Physics, Panjab University, Chandigarh 160 014, India*
[2]*Nuclear Science Centre, New Delhi 110 067, India*
(Received 29 January 2001; published 10 December 2001)

The elastic and inelastic scattering cross sections of 28.0 MeV protons on ^{56}Fe are measured. The results are analyzed in the framework of the coupled channels formalism. The nucleus ^{56}Fe has been described in the literature to be soft regarding vibrational as well as asymmetric rotational motion. The analysis has therefore been done in terms of two collective models, i.e., the harmonic vibrational model and the asymmetric rotor model. In the vibrational model it was necessary to include the one-phonon components in the wave functions of the two-phonon 2^+ and 4^+ states while in the asymmetric rotor model the contributions due to the higher multipole moments (β_{40},β_{42}) were found to be significant in the excitation of the 4_1^+ and 4_2^+ states.

DOI: 10.1103/PhysRevC.65.014305 PACS number(s): 25.40.Ep, 21.10.Re, 27.40.+z

INTRODUCTION

The low-lying levels of nuclei in the $1f$-$2p$ shell region manifest the collective features intermediate between the harmonic vibrators and the rigid rotors. This behavior is born out by the enhanced electromagnetic transition probabilities and the large static quadrupole moments for the first few excited states. The static moments provide a sensitive measure for the deformation of the nuclear surface. The measurements of the static quadrupole moments of ^{56}Fe and ^{58}Fe indicate the prolate deformation for these two nuclei [1–3]. The $BE(2)$ values for the $2_1^+ \rightarrow 0_1^+$ and $4_1^+ \rightarrow 2_1^+$ transitions are large which indicate these nuclei to have the collective excitations [4,5]. Ballester *et al.* [6] have reported the results of the inelastic scattering of 25 MeV α particles on ^{56,58}Fe. They analyzed the data with the coupled channel method and tried to reproduce the angular distributions of the 2_1^+, 2_2^+, 4_1^+, and 4_2^+ states within the framework of the asymmetric rotational model (ARM) and 2_1^+, 2_2^+, 4_1^+, and 3_1^- excited states in the framework of the harmonic vibrational model (HVM). Their results for higher states were not reliable due to the poor energy resolution (250 keV) of the detector and the large statistical errors.

De Leo *et al.* [7] have investigated the low-lying states in ^{56}Fe by means of inelastic proton and deuteron scattering experiments. The scattered particles have been analyzed by using the magnetic spectrograph. They extracted the negative values of the deformation parameters in the framework of coupled channel calculations indicating an oblate deformation for this nucleus, while the value of the deformation parameters given by Ballester *et al.* for the 2_1^+ state indicated a prolate deformation. We have therefore analyzed the data to remove the present ambiguity about prolate or oblate deformation and to get the information regarding the higher multipole moments in this nucleus. In this work we could resolve the 4_2^+ and 2_3^+ states due to the better energy resolution (50 keV) and statistics.

EXPERIMENTAL METHOD

The 28 MeV proton beam from the 15 UD Pelletrn at NSC, New Delhi, was used for the present experiment. Rolled self-supporting 850-μg/cm^2-thick spectroscopically pure metal foil of the natural iron (91.8% ^{56}Fe) was used as the target. The scattered protons were detected with a (ΔE $-E$) telescope consisting of 300-μm ΔE surface barrier detector and 5-mm Si(Li) detector. The angular distribution was measured in the angular range between 28.5 and 65° in steps of 2.5°. Figure 1 shows a typical proton energy spectrum of the outgoing protons at 62.5°. At forward angles, the contamination peaks from ^{12}C and ^{16}O were present but were clearly separated from the peaks of interest.

COUPLED CHANNEL ANALYSIS AND RESULTS

Elastic scattering

The first step was to search for a set of optical model parameters to fit the experimental elastic cross section using the Woods-Saxon form of the optical potential as given below:

$$V(r) = (-V + iW_s)(1+e)^{-1} - i4a_i W_D \cdot d/dr(1+e)^{-1} + V_{LS}(\hbar/m_\pi c)^2 \cdot (L \cdot S) \cdot 1/r \cdot d/dr(1+e)^{-1} + V_{\text{coul}},$$

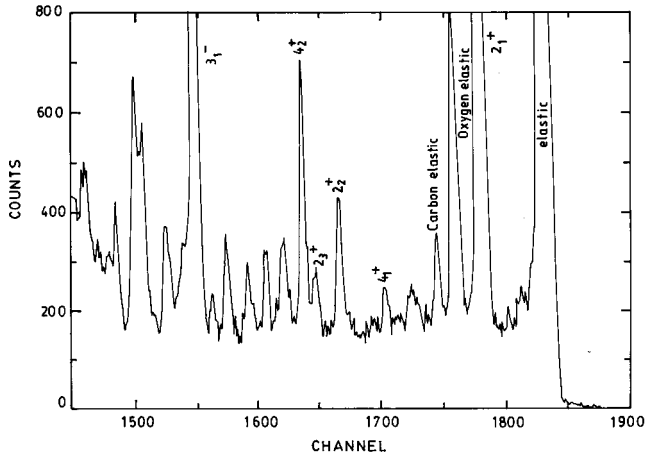

FIG. 1. A typical energy spectrum of the scattered protons from ^{56}Fe at θ=62.5°.

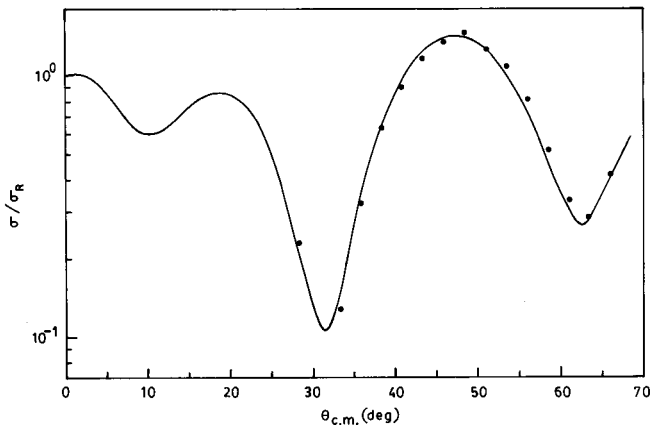

FIG. 2. The theoretical and experimental differential elastic scattering cross section for the 28.0 MeV protons from the ^{56}Fe.

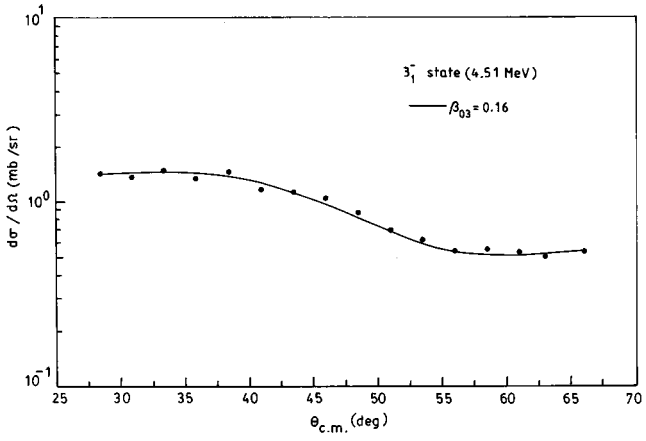

FIG. 3. The experimental and theoretical differential inelastic scattering cross sections for the 3_1^- state with $\beta_{03}=0.16$.

where

$$e=\exp\{[r-R(\theta',\phi')]/a\}.$$

The initial fitting was made by the starting values of optical potential parameters for protons from Perey and Perey [8] but the final values of the parameters were obtained by fine tunning of the parameters to fit the elastic scattering cross sections. Figure 2 shows the best fit of the experimental elastic scattering cross section using the final optical model parameters given in Table I. The coupling to the 2_1^+ state was included while calculating the elastic cross sections. The details of the fitting procedure are given elsewhere [9].

Inelastic scattering

The calculations of the differential cross sections for the various excited states were performed by a coupled channel method using the computer code ECIS88 [10,11]. The large static quadrupole moments and enhanced transition probabilities are the signature of the rotational behavior of the ^{56}Fe but the excitation of the 3_1^- (4.51 MeV) state is a typical signature of the vibrational nature. Due to the co-existence of the rotational and vibrational motions, the inelastic scattering data was analyzed both in terms of the ARM and the HVM prescriptions.

Vibrational model

In the vibrational model the 2_1^+ (0.846 MeV) state was analyzed considering it as a one phonon quadrupole state. The value of the β_{02} was deduced to be $+0.19$ which is consistent with the earlier measurement of Ballester *et al.* [6] indicating a prolate deformation of this state. The 3_1^- state was analyzed in terms of the octupole one phonon transition $(0_1^+ \rightarrow 3_1^-)$ and the phonon amplitude β_{03} was found to be equal to 0.16. As shown in Fig. 3, the HVM gives a good description for the 3_1^- state.

TABLE I. Proton optical model potential parameters.

Potential	Depth (MeV)	Radius	Diffuseness
Real	54.73	1.100	0.813
Volume imaginary	9.39	1.370	0.516
Surface imaginary	1.51	1.370	0.516
Real spin orbit	4.73	1.142	0.433
Coulomb		1.110	

An attempt to describe the 2_2^+ state (2.657 MeV) by HVM considering this to be a pure two phonon state with $\beta_2=0.19$ was not successful. The calculated angular distribution for this state was much smaller than the experimental one. As the next step, we used the anharmonic vibrational model (AVM) to reproduce the experimental cross section of the 2_2^+ level. According to Tamura [12], the observed anharmonicities are accounted for by assuming the wave function to be composed of both the two phonon and the one phonon amplitudes,

$$|I\rangle=\sin\gamma_I|\rangle I_{2ph}+\cos\gamma_I|\rangle I_{1ph},$$

where γ_I is the mixing angle which determines the relative contribution of the one and the two phonon amplitudes. The deformations are written as

$$\beta_{2I}=\beta_{02}\sin\gamma_I,$$

$$\beta_{0I''}=\beta_{0I}\cos\gamma_I,$$

where β_{2I} represents the amplitude of the one phonon transition from 2_1^+ to two phonon states of angular momentum I and $\beta_{0I''}$ represents the one phonon amplitude from the ground state to the two phonon states with angular momentum I, while β_{02} represents the one phonon amplitude from 0_1^+ to 2_1^+ state in the pure HVM.

The experimental angular distributions of the 2_2^+ state (2.657 MeV) and 2_3^+ (2.96 MeV) states were analyzed as two phonon state with a one phonon mixing. These fits are shown in Fig. 4 and the values of the resulting deformation parameters are tabulated in Table II. Our results for the deformation parameters of the 2_2^+ and 2_3^+ states are more in agreement with the results of De Leo *et al.* except the sign of the deformation.

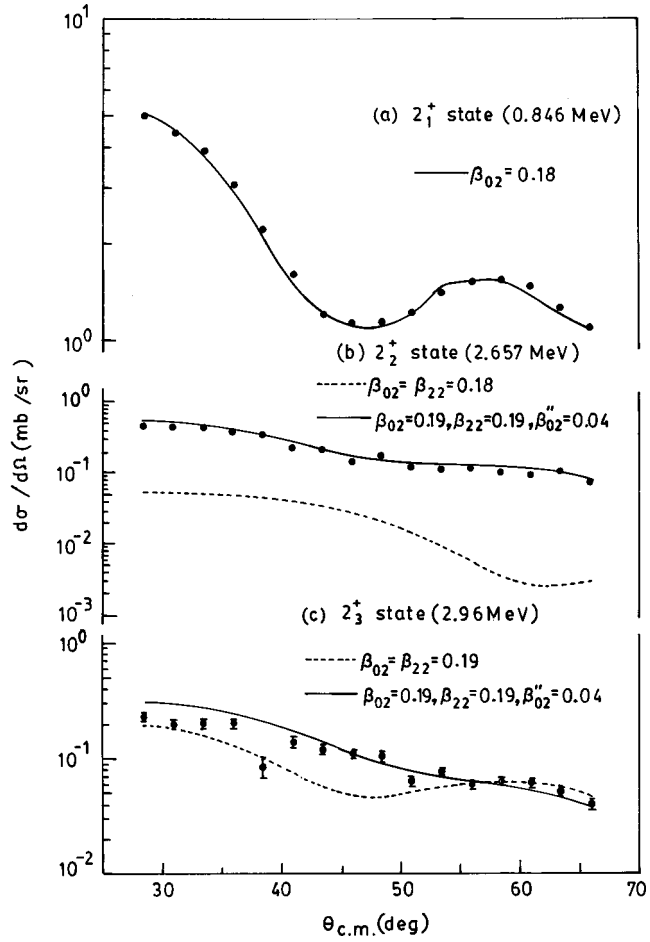

FIG. 4. The experimental and theoretical inelastic scattering cross sections (a) for the 2_1^+ state, solid curve is the first order HVM calculations with $\beta_{02}=0.19$ (b) same for the 2_2^+ state, dashed curve represents the first order HVM calculations (0_1^+-2_1^+-2_2^+) with $\beta_{02}=\beta_{22}=0.19$, while solid curve represents AVM calculations (0_1^+-2_1^+-2_2^+) with $\beta_{02}=0.19$, $\beta_{22}=0.18$, and $\beta''_{02}=0.04$. (c) same for 2_3^+ state, dashed curve represents the first order HVM (0_1^+-2_2^+-2_3^+) with $\beta_{02}=\beta_{22}=0.19$ and solid curve represents the AVM calculations with $\beta_{02}=0.19$, $\beta_{22}=0.18$. and $\beta_{02}=0.04$.

Hexadecapole-vibrational state

In addition to the quadrupole and octupole one-phonon states, the 4_1^+ state (2.085 MeV) and the strongly excited 4_2^+ state (3.123 MeV) were also analyzed as a mixture of two phonon quadrupole and one phonon hexadecapole excitation. The coupled channel calculations for these states are shown in Fig. 5 with $\beta_{04}(4_1^+)=0.02$ and $\beta_{04}(4_2^+)=0.09$. Table II shows the comparison of our results with the data obtained earlier. Our results for the 4_1^+ and 4_2^+ states are in agreement with the results of De Leo *et al.* within the experimental errors except the sign of deformation which is found to be positive in our case.

TABLE II. Deformation parameters of ^{56}Fe obtained with vibrational model CC calculations.

Transitions	Deformations	Present result	Ref. [6]	Ref. [7]
gs-2_1^+	β_{02}	0.19(2)	0.20	−0.218(7)
gs-2_2^+	$\beta_{02''}$	0.04(1)	−0.06	−0.049(3)
gs-2_3^+	$\beta_{02''}$	0.04(1)		−0.029(2)
gs-4_1^+	$\beta_{04''}$	0.02(1)		−0.016(4)
gs-4_2^+	$\beta_{04''}$	0.09(1)		−0.088(5)
gs-3_1^-	β_{03}	0.16(2)	0.15	−0.156(9)

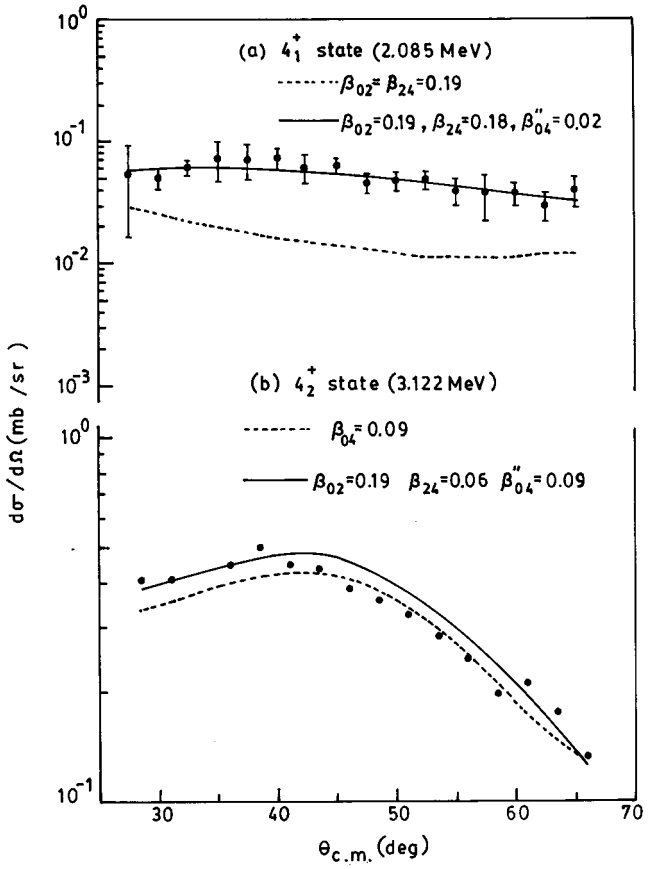

FIG. 5. The experimental and theoretical differential inelastic scattering cross sections (a) for the 4_1^+ state, dashed curve represents the first order HVM calculations ($0-2-4$) with $\beta_{02}=\beta_{24}=0.19$ and solid curve represents the AVM calculations ($0-2-4$) with $\beta_{02}=0.19$, $\beta_{24}=0.18$, and $\beta''_{04}=0.02$. (b) Same for the 4_2^+ state, dotted curve represents the first order HVM calculations ($0_1^+-4_2^+$) with $\beta_{04}=0.09$ and solid curve represents the AVM calculations ($0_1^+-2_1^+-4_2^+$) with $\beta_{02}=0.19$, $\beta_{24}=0.06$, and $\beta''_{04}=0.09$.

ASYMMETRIC ROTATIONAL MODEL

The nucleus ^{56}Fe also shows some of the properties of a permanently deformed asymmetric shape, therefore the excitation of the low-lying states may also be treated within the framework of the asymmetric rotor model [13,14]. In this model the shape of the nucleus is given by

$$R(\Omega')=R_0(1+\Sigma_{\lambda\mu}\beta_{\lambda\mu}Y_{\lambda\mu}(\Omega')$$

with

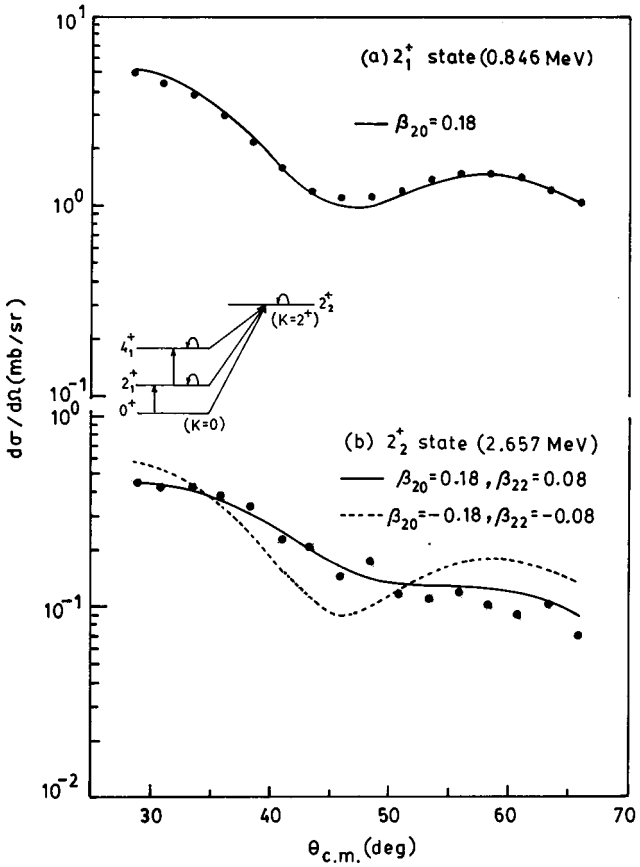

FIG. 6. The experimental differential inelastic scattering cross sections and the coupled channel ARM calculations with $(0_1^+\text{-}2_1^+\text{-}2_2^+\text{-}4_1^+)$ couplings (a) for the 2_1^+ state with $\beta_{20}=0.18$ (b) for the 2_2^+ state with $\beta_{20}=0.18$ and $\beta_{22}=0.08$ (solid line) and $\beta_{20}=-0.18$ and $\beta_{22}=-0.08$ for (dashed line).

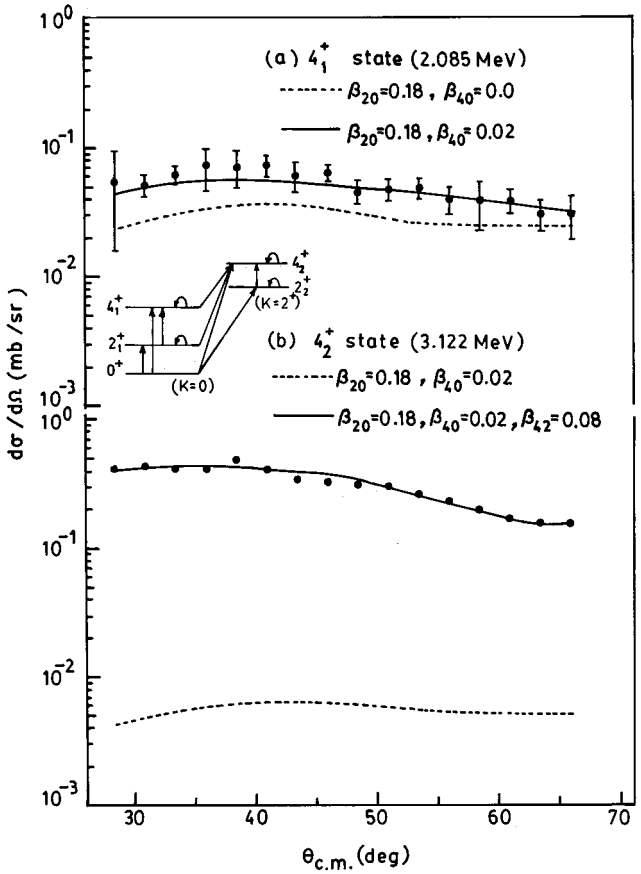

FIG. 7. The experimental differential inelastic scattering cross section and the coupled channel ARM calculations with $(0_1^+\text{-}2_1^+\text{-}2_2^+\text{-}4_1^+\text{-}4_2^+)$ couplings (a) for the 4_1^+ state, dashed curve with $\beta_{20}=0.18$ and $\beta_{40}=0.0$; solid curve with $\beta_{20}=0.18$ and $\beta_{40}=0.02$ (b) same for the 4_2^+ state, dashed curve with $\beta_{20}=0.18$, $\beta_{40}=0.02$, $\beta_{42}=0.0$ and solid curve with $\beta_{20}=0.18$, $\beta_{40}=0.02$, and $\beta_{42}=0.08$.

$$\beta_{\lambda\mu}=\beta_{\lambda-\mu}.$$

For quadrupole deformation

$$\beta_{20}=\beta_2\cos\gamma_2,$$

$$\beta_{22}=\beta_{2-2}=1/\sqrt{2}\beta_2\sin\gamma_2.$$

For hexadecapole deformation

$$\beta_{40}=\beta_4\cos\gamma_3,$$

$$\beta_{42}=\beta_{4-2}=1/\sqrt{2}\beta_4\sin\gamma_3\cos\gamma_4,$$

$$\beta_{44}=\beta_{4-4}=1/\sqrt{2}\beta_4\sin\gamma_3\sin\gamma_4.$$

The parameters γ_3 and γ_4 depend on the amplitude of the direct transitions from the ground state to three 4^+ states of $K^\pi=0^+$, 2^+, and 4^+ bands.

Ground-state band

In this band we could resolve 2_1^+ and 4_1^+ states clearly. We analyzed the 2_1^+ state with the coupling scheme $0_1^+\text{-}2_1^+\text{-}2_2^+\text{-}4_1^+\text{-}4_2^+$. The 2_1^+ state was well reproduced with $\beta_2=0.18$ as shown in Fig. 6(a) which is in agreement with the result of Ballester *et al.* The experimental cross sections for the 4_1^+ state were fitted by introducing the β_{40} term in the optical model potential with $\beta_{40}=0.02$ as shown in Fig. 7(a).

γ band ($K\pi^+=2^+$)

We considered the 2_2^+ state as a band head of the $K=2^+$ γ band. The nuclear shapes in the ARM are defined in terms of the β and γ values. Using the $0_1^+\text{-}2_1^+\text{-}2_2^+\text{-}4_1^+\text{-}4_2^+$ coupling channels, the best fit was obtained with $\beta_2=0.20$ and $\gamma=24.5°$ for the 2_1^+ and 2_2^+ states as shown in Fig. 6(b). One can see that $\beta_2<0$ does not reproduce the 2_2^+ data as predicted by Ballester *et al.* It is important to note that we need to introduce a comparatively larger value of the β_{42} equal to 0.08 to reproduce the data of the 4_2^+ state as shown in Fig. 7(b). The deformation parameters obtained for the different excited levels are tabulated in Table III. It is significant to note that the β_{42} value (0.08) was found to be roughly four times larger as compared to β_{40} (0.02). Ballester *et al.* without including the β_{42} deformation, have reproduced the

TABLE III. Deformation parameters of ^{56}Fe obtained by asymmetric rotational model.

Parameters	Present work	Ref. [6]
β_{20}	0.18(2)	0.17
β_{22}	0.08(1)	
β_{40}	0.02(1)	
β_{42}	0.08(1)	0.065

4_2^+ state by including only $\beta_{40}Y_{40}$ term in the potential with $\beta_4=0.065$, but this value of β_4 has overpredicted the cross sections for the 4_1^+ state by about ten times. However, our values of β_{40} and β_{42} are consistent (except the sign of deformation) with the values obtained by De Leo *et al.* with the vibrational model including one phonon transition from the ground state. This behavior of a large β_{42} value, typical for the nuclei soft to γ vibrations, was also seen earlier in the rare earth nuclei [15].

CONCLUSION

The proton elastic and inelastic differential cross sections of the 0_1^+ ground state and 2_1^+, 2_2^+, 2_3^+, 3_1^-, 4_1^+, and 4_2^+ excited states have been analyzed in the framework of the coupled channel formalism using the anharmonic vibrational model and the asymmetric rotor model. The values obtained for the deformation parameters from the two models are close within the experimental errors. The 2_1^+ and 3_1^- states data was well reproduced by the first order HVM but to reproduce the angular distributions of 2_2^+, 2_3^+, 4_1^+, and 4_2^+ states, it was necessary to consider the admixture of one phonon direct excitation to these states besides the two phonon components in the vibrational wave functions.

The ARM, on the other hand, reproduces the angular distributions of the 0_1^+, 2_1^+, 2_2^+, 4_1^+, and 4_2^+ states with the introduction of the higher multipole deformations β_{40} and β_{42}. The values of $\beta_{42}=0.08$ was found to be significantly larger as compared to $\beta_{40}=0.02$ for this nucleus. This was observed earlier in ^{168}Er nucleus also and therefore seems to be characterstic of the nuclei which are soft to the γ deformation. Our results for hexadecapole strength for 4_1^+ and 4_2^+ states and quadrupole strength for 2_1^+, 2_2^+, and 2_3^+ states are in agreement with the results of De Leo *et al.* but differ in sign indicating the prolate deformation for these states rather than the oblate deformation as predicted by him.

ACKNOWLEDGMENTS

The authors acknowledge with thanks the University Grants Commission (UGC) for financial support and the Pelletron accelerator crew of NSC New Delhi for providing an excellent beam during the experiment.

[1] J. A. Thomson, R. P. Scharenberg, and W. R. Lutz, Phys. Rev. **4**, 1699 (1971).
[2] P. M. S. Lesser, D. Cline, Philip, and R. N. Horoshko, Nucl. Phys. **A190**, 597 (1972).
[3] M. J. Levine, E. K. Warburton, and D. Schwalm, Phys. Rev. C **23**, 244 (1981).
[4] Huo Junde, Hu Dialing, Zhou Chunmei, Han Xiaoling, Hu Baohua, and Wu Yaodong, Nucl. Data Sheets **51**, 1 (1987), and references therein.
[5] L. K. Perker, Nucl. Data Sheets **42**, 457 (1984), and references therein.
[6] F. Ballester, E. Casal, and J. B. A. England, Nucl. Phys. **A501**, 301 (1989).
[7] R. De Leo *et al.* Phys. Rev. C **53**, 2718 (1998).
[8] C. M. Perey and F. G. Perey, At. Data Nucl. Data Tables **13**, 293 (1974).
[9] I. M. Govil, H. W. Fullbright, and D. Cline, Phys. Rev. C **36**, 1442 (1987).
[10] J. Raynal, Phys. Rev. C **23**, 2571 (1981).
[11] J. Raynal, in *Computing as a Language in Physics* (IAEA, Vienna, 1972).
[12] T. Tamura, Rev. Mod. Phys. **37**, 679 (1965).
[13] A. S. Davydov and G. F. Filippov, Nucl. Phys. **8**, 237 (1958).
[14] A. S. Davydov and V. S. Rostovsky, Nucl. Phys. **12**, 58 (1959).
[15] I. M. Govil *et al.* Phys. Rev. C **33**, 793 (1986).